CJC Chinese Journal of Chemistry 中国化学 · An International Journal

For submission: https://mc.manuscriptcentral.com/cjoc
For published articles: https://onlinelibrary.wiley.com/journal/16147065

Concise Report

Cite this paper: *Chin. J. Chem.* **2022**, *40*, 1156–1164. **DOI: 10.1002/cjoc.202100901**

A Rhein-Based Rh(III) Arene Complex with Anti-tumor Cell Proliferative Activity Inhibits RNA Demethylase FTO

Lu Liu,[‡,a,b] Yaqiong Kong,[‡,a] Liang He,[c] Xiuxiu Wang,[d] Meng-Meng Wang,[a] Hongjiao Xu,[b] Cai-Guang Yang,[b,e] Zhi Su,*[,a] Jing Zhao,*[,d] Zong-Wan Mao,*[,c] Yue Huang,*[,b,e] and Hong-Ke Liu*[,a]

[a] *School of Chemistry and Materials Science, Nanjing Normal University, Nanjing, Jiangsu 210023, China*
[b] *State Key Laboratory of Drug Research, Shanghai Institute of Materia Medica, Chinese Academy of Sciences, Shanghai 201203, China*
[c] *School of Chemistry, Sun Yat-Sen University, Guangzhou, Guangdong 510275, China*
[d] *School of Chemistry and Chemical Engineering, Nanjing University, Nanjing, Jiangsu 210023, China*
[e] *School of Pharmaceutical Science and Technology, Hangzhou Institute for Advanced Study, University of Chinese Academy of Sciences, Hangzhou, Zhejiang 310024, China*

Comprehensive Summary

Metallodrugs with fine-tuned coordination between metals and bioactive ligands can achieve cytotoxic effects in cancer therapy and have been considered as a new approach for drug design. However, it has yet to be elucidated whether these metallodrugs target epitranscriptomic proteins for gene expression regulation. This report describes a rhein-based Rh(III)-arene complex, Rh1, that exhibited promising antiproliferative effects in several tumor cell lines. Rh1 induced cell death through the autophagy, cell cycle arrest, and accumulation of intracellular reactive oxygen species (ROS). In addition, Rh1 upregulated the global N^6-methyladenosine (m^6A) levels in A549 cells in the fat mass- and obesity-associated protein (FTO)-dependent manner. Collectively, the metal-based FTO inhibitor Rh1 effectively suppressed tumor cell proliferation and modulated the abundance of cellular m^6A, highlighting the potential of metal-based agents to target and regulate epitranscriptomics for tumor suppression.

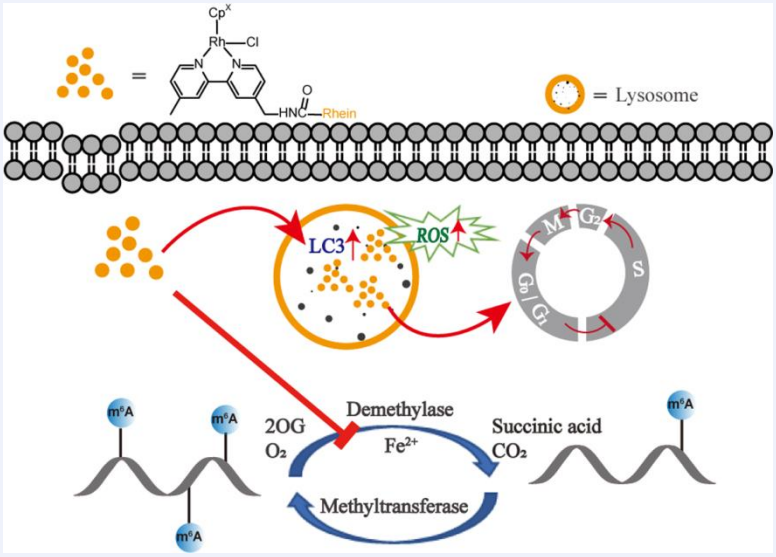

Keywords

Rhodium | mRNA | Antiproliferation | FTO | m^6A

*E-mail: liuhongke@njnu.edu.cn, huangyue@simm.ac.cn, cesmzw@mail.sysu.edu.cn, jingzhao@nju.edu.cn, zhisu@njnu.edu.cn
[‡] These authors contributed equally to this work.

View HTML Article | Supporting Information

Background and Originality Content

Coordination complexes incorporating metal ions with biologically active ligands have been broadly used as diagnostic tools, anticancer drugs, and bioimaging agents.[1] Cisplatin, as a landmark discovery of metal complexes, has been used clinically for treating numerous human cancers.[2] However, drug resistance and undesirable side effects of cisplatin have led to other platinum-containing anticancer drugs or combination therapies of cisplatin with other drugs being considered as novel strategies for chemotherapy.[3] In recent years, coordination complexes with several transition metals have attracted increasing attention because of their variable oxidation states, higher selectivity for cancer cells, and iron mimicking properties.[4] The ruthenium (Ru) complexes KP1019 and NAMI-A progressed to clinical trials, but these were terminated for various reasons.[5] Diverse approaches such as novel scaffold incorporation, light activation, catalytic mechanisms of action, and pH-dependent modulation of reactivity have been applied for the design of metallodrugs.[6] The half-sandwich arene complexes coordinated with metal centers such as rhodium (Rh) and iridium (Ir) and ancillary ligands play synergistic roles in fine-tuning the *in vitro* and *in vivo* anticancer properties of the compounds.[7] However, further work is required to understand the mechanisms of the anticancer activity.

Early mechanistic studies demonstrated that the half-sandwich metal-arene complexes interacted with the N7 of guanine, similar to the interaction of cisplatin with DNA, and this was believed to be one of the main causes of the anticancer activity.[8-9] Recent studies revealed that enzymes were the potential binding targets for the metal-arene complexes.[10] Several classes of proteins with different roles, including kinases and DNA-repair proteins have been characterized as the targets of metallodrugs *in vitro* and *in vivo*.[11] Using an integrated proteomics-based target-response profiling approach, a series of Ru(II)-arene (RAPTA) compounds were determined to inhibit thioredoxin reductase and cathepsin B,[12] or mainly target the cytoskeletal protein plectin to affect the motility of cancer cells.[13] In addition, metal-based inhibitors have been developed to selectively target the histone deacetylases (HDACs) to modulate the epigenetic status and achieve the anticancer effect.[14]

The rich photophysical properties and unique optical parameters of the metal complexes mean cellular imaging can be used to elucidate the various biological processes and *in vivo* trafficking of these drugs.[15] Subsequently, organelle-targeting strategies have been applied to improve the anticancer therapeutic effects by delivering the metallodrugs to specific cell compartments such as the nucleus, mitochondria, and lysosomes.[16] For example, some Ir(III) complexes were reported to accumulate in lysosomes, leading to lysosomal damage and induction of autophagy or apoptosis.[17] Other metal complexes tended to locate in mitochondria and induced caspase-dependent apoptosis by mitochondrial damage, cellular ATP depletion, mitochondrial respiratory inhibition, and elevated production of reactive oxygen species (ROS).[18-19] Furthermore, some metal complexes escaped and migrated to other organelles once stimulated by photoirradiation to produce ROS.[20] Therefore, such targeted luminescent metal complexes provide a structural foundation for the further design and optimization of metallodrugs.

In this study, rhein, a reported inhibitor for the fat mass- and obesity-associated protein (FTO),[21] which was identified as a critical demethylases involved in regulating cellular mRNA stability by erasing m^6A from mRNA,[22] was taken as the ligand and used to develop the first example of a rhein-based Rh(III) arene complex that maintained the inhibitory activity for FTO demethylation. The complex, termed Rh1, exhibited FTO-dependent antiproliferative activity by upregulating the global N^6-methyladenosine (m^6A) levels in A549 cells. In addition, Rh1 induced cell death through autophagy, cell cycle arrest, and the generation of intracellular ROS. These findings offer a new insight of metal-based complexes targeting the FTO demethylase for tumor suppression.

Results and Discussion

Chemical synthesis of the metal complexes Rh1 and Ru1

The half-sandwich organometallic Rh(III) complex Rh1 and Ru(II) complex Ru1 were synthesized by refluxing the ligand Rhein-L with the dimer $[(\eta^5\text{-}Cp^X)RhCl_2]_2$ (Cp^X = pentamethylcyclopentadienyl ($RhCp^X$) and $[(\eta^6\text{-}p\text{-cymene})RuCl_2]_2$ (Rucym), respectively (Schemes 1 & S1). The ligand Rhein-L and complexes of Rh1 and Ru1 were fully characterized with proton nuclear magnetic resonance (^1H NMR) spectroscopy and electrospray ionization mass spectrometry (ESI-MS) (Figures S1—S3).

Photophysical properties of Rhein-L, Rh1, and Ru1 were studied in DMSO/H_2O solution (*V*/*V*, 1 : 99) at room temperature, and the three samples displayed similar UV absorption and fluorescence emission. The ligand Rhein-L exhibited maximum UV absorption at 438 nm and a photoluminescence emission band at 610 nm with excitation at 450 nm in the DMSO/H_2O solution at room temperature (Figure S4). The complexes Rh1 and Ru1 displayed two obvious UV absorptions around 300 nm and 425 nm (Figure S5); the high-energy bands (< 320 nm) could be assigned to the ligand-centred (LC) transitions, while the relatively low-energy band at ~425 nm could be ascribed to the contribution from both ligand-to-ligand charge transfer (LLCT) transitions and metal-to-ligand charge transfer (MLCT).

Rh1 exhibits enhanced cytotoxic activity versus its dimer and ligand in tumor cell lines

In vitro cytotoxicity of Rh1 and Ru1, their dimers RhCpX and Rucym, respectively, and the ligand Rhein-L against tumor cells was assessed using the cell lines human lung carcinoma A549, cisplatin-resistant A549 (A549R), human breast cancer MCF-7, epithelial ovarian carcinoma A2780, and acute promyelocytic leukemia NB4. Cisplatin was set as a positive control. Rh1 exhibited marked cytotoxicity towards the tested tumor cell lines and

Scheme 1 Chemical structures of Rhein-L, $RhCp^x$ dimer, Rh1 ($RhCp^X$-Rhein), Ru-cym dimer, and Ru1 (Ru-cym-Rhein)

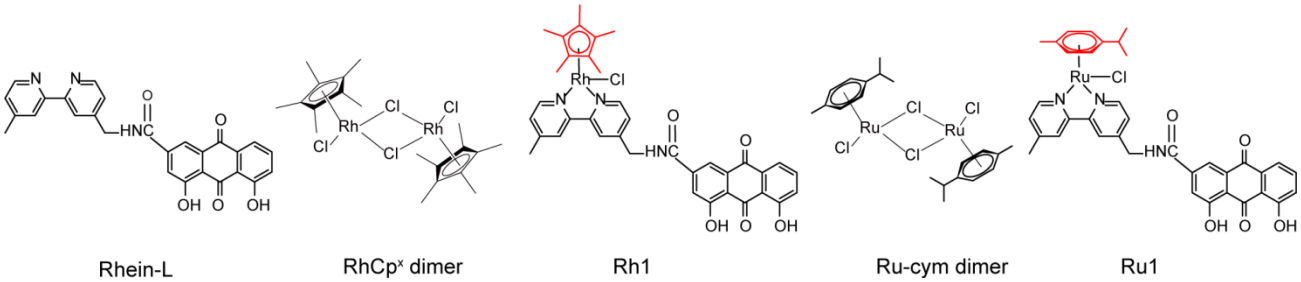

showed preferred antiproliferative activity in A549 and NB4 cells, with estimated IC_{50} values of 3.0 μmol/L and 2.3 μmol/L, respectively (Table S1). Rh1 also demonstrated the potency to overcome the cisplatin resistance in A549R cells, with IC_{50} values of 3.0 μmol/L and 8.8 μmol/L for A549 and A549R cells, respectively. In contrast, the cytotoxic/antiproliferative effects of the ligand Rhein-L were almost abolished in A549R cells (IC_{50} of 3.9 μmol/L for A549 and 35.0 μmol/L for A549R, respectively). Ru1 exhibited only moderate activity against tumor cells, with IC_{50} values greater than 15 μmol/L for all tested cell lines. Compared with the RhCpX dimer, Rhein-L, and Ru1 complex, Rh1 displayed the best efficacy for inhibiting the viability of A549 cells (Figure 1A). Furthermore, Rh1 significantly inhibited colony formation in A549 cells (Figure 1B). Based on these findings, Rh1 was selected for further investigation.

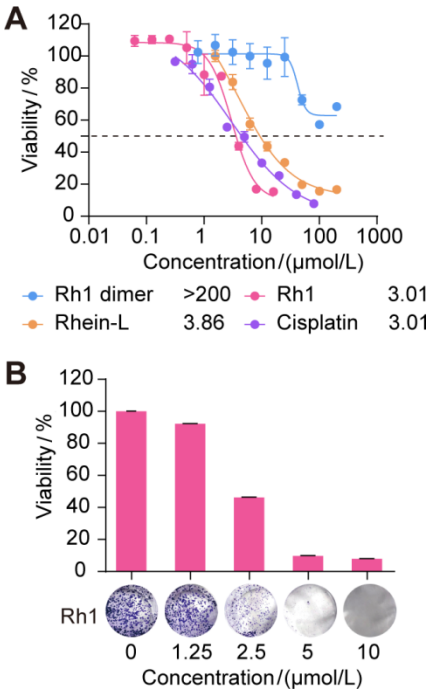

Figure 1 Rh1 exhibits an antiproliferative effect in A549 cells. (A) IC_{50} values of Rh1 dimer ($RhCp^X$), Rhein-L, Rh1, and cisplatin for inhibiting cell viability of A549 cells. (B) Effects of Rh1 on colony formation of A549 cells.

Rh1 accumulates in the lysosomes of A549 cells and leads to autophagic cell death

To understand the subcellular accumulation of Rh1, immunofluorescence staining was performed on A549 cells after incubation with Rh1. Fluorescence microscopy examination of the cells revealed that Rh1 exhibited a green fluorescence that merged with the lysosome dye LysoTracker Red (LTR), suggesting that Rh1 predominantly localized in the lysosomes (Figure 2A). Autophagy is an evolutionarily conserved stress-responsive process that culminates with the lysosomal degradation of redundant or potentially dangerous cytosolic entities.[23] The accumulation of LC3 puncta and the transformation from LC3-I to LC3-II were used as typical biomarkers to monitor autophagic responses in the cells.[24] Western blotting showed that endogenous LC3-II increased dose dependently upon Rh1 treatment over 24 h in A549 cells (Figure 2B), indicating that Rh1 induced an autophagy phenotype. Immunofluorescence assessment of LC3-II demonstrated that LC3-positive puncta were significantly elevated upon treatment with Rh1, manifesting the emergence of autophagosome vacuoles (Figure 2C). These observations suggested that treatment with Rh1 caused autophagic cell death in A549 cells.

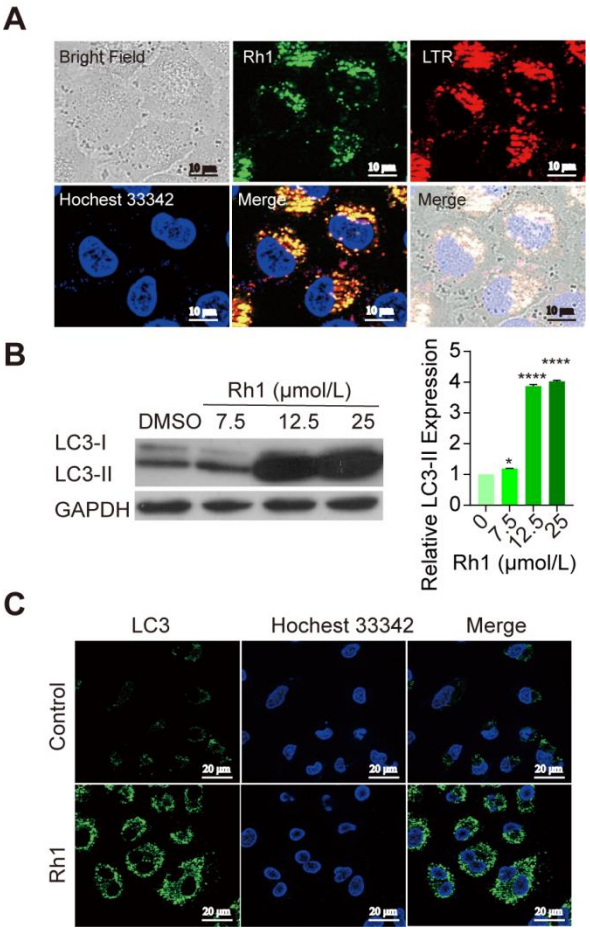

Figure 2 Rh1 accumulates in the lysosome and induces an autophagy phenotype in A549 cells. (A) Intracellular colocalization of Rh1 with LysoTracker Red (LTR) and Hoechst 33342. The excitation wavelengths for Rh1, LTR, and Hoechst 33342 were 405 nm, 357 nm, and 633 nm, respectively, and the emitted fluorescence was collected at 600 ± 20 nm, 660 ± 20 nm, and 460 ± 20 nm, respectively. Scale bar, 10 μm. (B) LC3 protein expression in A549 cells after Rh1 treatment. LC3 expression was analyzed by western blotting (left panel) and quantified with Image J software (right panel). (C) Immunofluorescence imaging of LC3 in A549 cells pre-treated with 10 μmol/L Rh1 for 12 h. Scale bar, 20 μm. ****, $p < 0.0001$.

Rh1 induces the intracellular ROS generation and cell cycle arrest

The excessive generation of ROS is an important mechanism for the metal-based anticancer agents and has also been reported to induce autophagy.[25] The generation of ROS in A549 cells was detected by using the fluorescent probe DCFH-DA (2',7'-dichlorofluorescin diacetate).[26] The number of fluorescence dots present with DCFH-DA probing was significantly increased in the A549 cells exposed to Rh1 treatment (Figure 3A). Moreover, the fluorescence intensity was enhanced in a time-dependent manner (Figure 3B). Thus, the Rh1 complex effectively induced the generation of intracellular ROS.

Increasing evidence suggests that autophagy and the cell cycle are coordinated and reciprocally regulated.[27] The effect of Rh1 treatment on cell cycle distribution in A549 cells was examined by propidium iodide (PI)/RNase staining and subsequent flow cytometry analysis. Rh1 could induce G0/G1 cell cycle arrest in a dose-dependent manner (Figures 3C and S6) and the proportion of A549 cells in G0/G1 phase increased from 57.16% to 77.46% after Rh1 treatment for 24 h. Collectively, these data demonstrated that Rh1 accumulates in lysosomes, induces ROS produc-

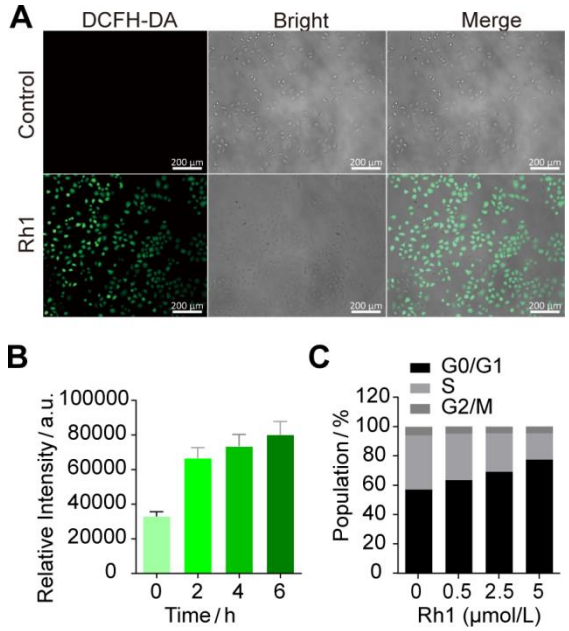

Figure 3 Rh1 induces excessive ROS production and cell-cycle arrest in A549 cells. (A) Fluorescence microscopy images of intracellular ROS production in A549 cells treated with 10 μmol/L Rh1. Scale bar, 200 μm. (B) Time-dependent ROS production measured with a fluorescence spectrometer. (C) Effects of Rh1 treatment on cell-cycle distribution using flow cytometry.

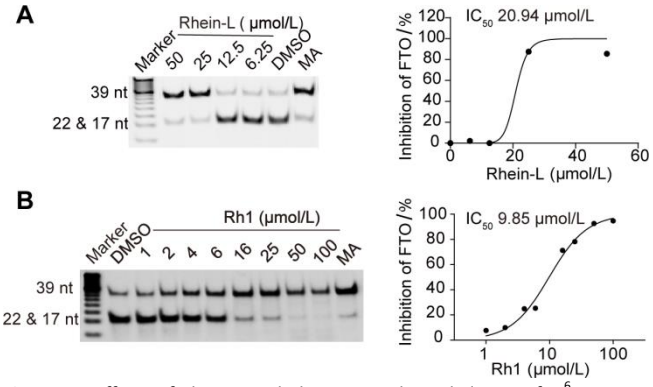

Figure 4 Effects of Rhein-L and Rh1 on FTO demethylation of m^6A *in vitro*. (A and B) Detection of Rhein-L (A) and Rh1 (B) inhibition of FTO demethylation on ssDNA using the restriction enzyme digestion assay. In PAGE image (left panel), the upper band is 39-nt DNA with dm^6A incorporation, and the lower 22- and 17-nt bands represent the demethylated products after DpnII digestion. IC_{50} values of the inhibition curve were drawn using Image J quantification (right panel). Meclofenamic acid (MA) was used as a positive control of FTO inhibitor at 50 μmol/L.

tion, arrests the cell cycle at G0/G1 phase, and leads to cell death by autophagy in A549 cells.

Identification of the inhibition activity of Rh1 on FTO demethylation

Rhein was previously shown to be the first FTO inhibitor.[7] Therefore, the rhein-based complex Rh1 was examined to determine whether the complex retained the inhibitory activity on FTO demethylation. The demethylation activity of FTO was completely abolished in the presence of 50 μmol/L $RhCp^x$ dimer and Rh1, while Ru-cym dimer and Ru1 treatment displayed no inhibition activity under the same conditions (Figure S7A). The IC_{50} values of Rhein-L, Rh1, and the dimer $RhCp^x$, respectively, on FTO demethylation were quantified to further determine the inhibitory effects of the compounds. The IC_{50} values of Rhein-L and Rh1 for the inhibition of FTO demethylation were 20.9 μmol/L and 9.9 μmol/L, respectively (Figures 4A and 4B). Meanwhile, the $RhCp^x$ dimer exhibited enhanced FTO inhibition activities compared with Rhein-L or Rh1, with an IC_{50} value of 2.3 μmol/L (Figure S7). These results demonstrate that both $RhCp^x$ dimer and Rhein-L contribute to the inhibitory activity of FTO, and Ru1 does not show an inhibitory effect that may be attributed to Ru-cym dimer.

Rh1 exhibits FTO-dependent antiproliferative activity via the FTO/m^6A axis in A549 cells

To investigate whether Rh1 could alter the level of m^6A modification in A549 cells, the abundance of m^6A was investigated *in vitro* by dot blot assay under dose-dependent conditions. As expected, the m^6A abundance in total RNA and mRNA markedly increased after Rh1 treatment (Figures 5A and 5B). To further determine whether the inhibitory effect of Rh1 on cell proliferation relied on FTO, stable FTO knockdown (shFTO) A549 cells were generated with lentivirus-mediated shRNA. The efficacy of knockdown was confirmed by the expression levels of FTO protein and mRNA (Figures 5C and 5D). MTT and colony formation assays revealed that knockdown of FTO in A549 cells significantly suppressed cell proliferation (Figures 5E and 5F), indicating FTO as an oncogene in A549 cells, which was consistent with the reported results.[28-29] Rh1 markedly suppressed the proliferation of A549 cells but exhibited a much milder effect on A549 shFTO cells. The IC_{50} value of Rh1 for inhibiting the proliferation of A549 shNC (negative control) cells was 3.3 μmol/L, while the IC_{50} values for Rh1 on A549 shFTO-1 and shFTO-2 cells were 10.1 μmol/L and 10.4 μmol/L, respectively (Figure 5G). In addition, A549 shFTO cells showed significant dose-dependent drug sensitivity against Rh1 (Figure 5H), suggesting that the inhibitory effect of Rh1 on the proliferation of cells was dependent on FTO protein.

Further studies were performed to exclude the effects of Rh1 on methylation of histone and genomic DNA. Rh1 only minimally altered major histone methylations (Figure S8A) and genomic 5-methylcytosine (5mC) and 5-hydroxymethylcytosine (5hmC) modifications in A549 cells (Figure S8B). Collectively, Rh1 might achieve antitumor effects through targeting the FTO-mediated regulatory pathway of RNA demethylation rather than the epigenetic histone or DNA demethylation.

Conclusions

As a result of the clinical success of cisplatin in the early 1960s, considerable progress has been made with metal complexes for biological application in the past half century. However, drug resistance and undesirable side-effects of cisplatin are major obstacles in current clinical chemotherapy. To address these problems, novel elements such as new metal centers, ancillary ligands, and flexible scaffolds have been applied to the design of metal complexes to improve the biological activities. Furthermore, metal substitution or novel scaffold of complexes may facilitate the clinical introduction of the next generation of platinum or other metal-based anticancer agents. For the half-sandwich metal-arene complex, the arene moiety favors structural diversity and hydrophobicity, which not only provides additional functionalities but also facilitates cellular uptake by ameliorating lipophilicity. In the current study, a rhein-based Rh(III) arene complex, Rh1, was synthesized and found to significantly repress the proliferation of A549 cells, including those that were resistant to cisplatin (Figure 1 and Table S1). Similar to the classical metal complexes, Rh1 exerted antiproliferative effects on A549 cells by accumulating in lysosomes and inducing autophagy, arresting the cell cycle at G0/G1 phase, and significantly increasing the level of intracellular ROS (Figures 2 and 3). Rhein was originally used as a laxative and stomach drug and was reported as the first FTO inhibitor, so the

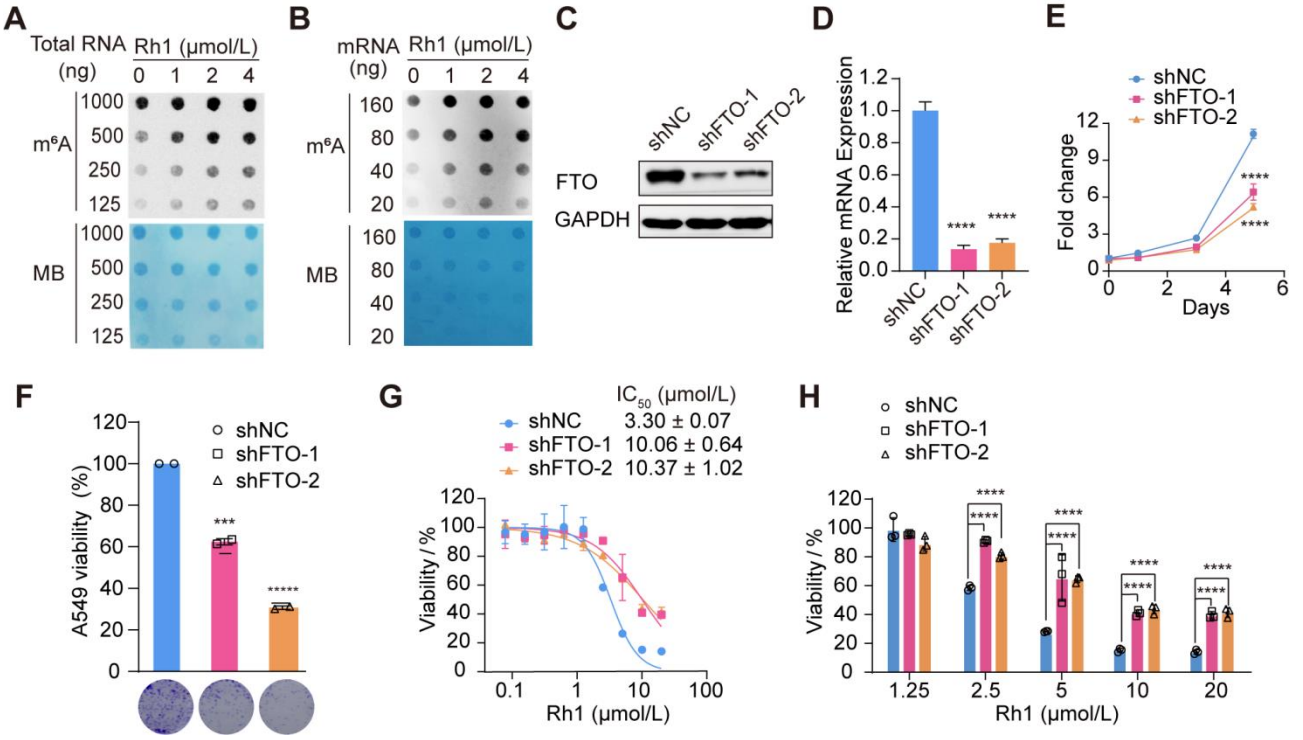

Figure 5 Rh1 exhibits FTO-dependent antiproliferative activity in A549 cells. (A and B) Dot blot assay determination of m^6A abundance in total RNA (A) and mRNA (B) in A549 cells treated with Rh1 for 48 h. MB (methylene blue) represents loading control of RNA samples. (C and D) The FTO protein (C) and mRNA (D) levels in A549 cells infected with lentivirus carrying indicated shRNAs. shNC, control cells. shFTO-1 or shFTO-2, FTO-knockdown cells. (E) Effects of shFTO on A549 cell viability. (F) Effects of shFTO on colony formation of A549 cells. (G) IC_{50} values of Rh1 for inhibiting cell viability in shNC and shFTO A549 cells. (H) Effects of indicated dosage of Rh1 on cell viability in shNC and shFTO A549 cells. ****, $p < 0.0001$; ***, $p < 0.001$.

inhibitory activity of Rh1 on FTO was then determined, indicating that Rh1 may possess different mechanisms of action. As expected, Rh1 maintained the inhibitory activity towards FTO demethylase. In addition, the RhCpX dimer exhibited the best inhibitory activity (Figures 4 and S7), which indicated the FTO inhibitory capability of Rh1 may arise from the synergy of the ligand Rhein-L and RhCpX dimers. However, the Rucym dimer did not show the inhibitory activity on FTO (the data are not shown) and inhibitory mechanism for the RhCpX dimer was unclear.

Antiproliferative effects on A549 cells by accumulating in lysosomes and inducing autophagy, arresting the cell cycle at G0/G1 phase, and significantly increasing the level of intracellular ROS (Figures 2 and 3). Rhein was originally used as a laxative and stomach drug and was reported as the first FTO inhibitor, so the inhibitory activity of Rh1 on FTO was then determined, indicating that Rh1 may possess different mechanisms of action. As expected, Rh1 maintained the inhibitory activity towards FTO demethylase. In addition, the $RhCp^X$ dimer exhibited the best inhibitory activity (Figures 4 and S7), which indicated the FTO inhibitory capability of Rh1 may arise from the synergy of the ligand Rhein-L and $RhCp^X$ dimers. However, the Ru-cym dimer did not show the inhibitory activity on FTO (the data are not shown) and inhibitory mechanism for the $RhCp^X$ dimer was unclear.

Several specific or non-specific small-molecule inhibitors of FTO have been identified and these can be classified into 2-oxoglutarate (2OG)-competitive, substrate competitive, dual 2OG- and substrate-competitive, and unvalidated mechanisms depending on their mode of action.[30] More recently, several small molecules, such as FB23-2, CS1, CS2, and Dac51, have been developed that exhibit clinical potential for cancer therapy by targeting FTO.[31-33] However, to our knowledge, no metal complex with FTO inhibitory activity has been characterized to date. The catalytic nanoparticles OsSx-PEG NPs were recently shown to increase the methylation level of mRNA, but the cellular target has yet to be elucidated.[34] The current study successfully synthesized a rhein-derived metal complex Rh1 with FTO inhibitory activity. Knocking down FTO expression with lentivirus revealed that FTO downregulation repressed the proliferation and colony formation of A549 cells, which was similar to the effects of Rh1 treatment. In addition, Rh1 significantly increased the m^6A abundance and exhibited FTO-dependent antiproliferative activity in A549 cells. Collectively, Rh1 was shown to suppress the proliferation of A549 cells by targeting the FTO/m^6A axis. Although more systematic studies are warranted to verify the involvement of Rh1 in FTO-regulated targets or pathways, this study has provided evidence that metal complexes targeting epitranscriptomics hold potential for tumor suppression.

Experimental

Materials

The m6A-containing ssDNA substrate was synthesized in Generay Company. The biological reagents for enzymatic assay such as Tris, α-ketoglutarate, $(NH_4)_2Fe(SO_4)_2$ and *L*-ascorbic acid were purchased from Shanghai Bioengineering Company. The components for cell cultures such as Dulbecco's Modified Eagle Medium (DMEM), RPMI1640 medium, Fetal Bovine Serum (FBS), penicillin/streptomycin and trypsin/EDTA solution were purchased from Gibco. The sodium of meclofenamic acid (MA) was obtained from TCI.

Instruments

ESI-MS was recorded by the Thermo LCQFLEET electrospray mass spectrometer. ^1H NMR was determined by Bruck AVANCE 400 MHz spectrometer, and the UV-visible spectra were collected by Varian Cary 50 Probe UV-vis spectrometer. The fluorescence spectrum was performed by Perkin-Elmer LS55 fluorescence

spectrometer, and the digital circular second spectrometer was using Chriascan instrument produced by Applied Photophysics Company in the United Kingdom. The multifunctional enzyme labeling instrument model was recorded by Tecan Infinite M1000 Pro, flow cytometry was SORP FACSARIA II, and the fluorescent microscope model was Axio Observer. CHI 660E electrochemical work station was used with a conventional three-electrode system.

Synthesis of ligand Rhein-L

The modified ligand (Rhein-L, 4, 5-dihydroxy-*N*-((4'-methyl-[2, 2'-bipyridin]-4-yl)methyl)-9,10-dioxo-9,10-dihydroanthracene-2-carboxamide) was synthesized from 4-aminomethyl-4-methyl-2,2-bipyridyl, which was prepared in a slightly modified way according to literature procedures.[35-36] Rhein (0.5 mmol), EDCI (0.5 mmol), HOBt (0.4 mmol), 4-aminomethyl-4-methyl-2,2-bipyridyl (2.0 mmol) and 10 μL triethylamine were mixed and kept at 0 °C for 10 h. Yellow precipitation was obtained after water was added, and further purified with the column chromatography (yield: 0.18 g, 78%). ^{1}H NMR (400 Hz, DMSO-d_6) δ: 11.93 (s, 2H), 9.66 (t, 1H), 8.63 (d, 1H), 8.52 (d, 1H), 8.38 (s, 1H), 8.28—8.22 (m, 2H), 7.85 (dd, 2H), 7.77 (d, 1H), 7.42 (t, 2H), 7.28 (d, 1H), 4.63 (d, 2H), 2.42 (s, 3H).

Synthesis of Rh1 and Ru1

The dimers $[(\eta^5\text{-Cp}^X)\text{RhCl}_2]_2$ (Cp^X = pentamethylcyclopentadienyl) or $[(\eta^6\text{-p-cymene})\text{RuCl}_2]_2$ (0.3 mmol) and Rhein-L (0.2 mmol) were mixed and stirred in CH_3OH at room temperature for 3 h. The solution was further concentrated by the rotary vacuum evaporation, and excessive NH_4PF_6 was added. The product could be filtered after frozen in the refrigerator.

Rh1 ($[(\eta^5\text{-CpX})\text{Rh(N^N-Rhein)Cl}]PF_6$) was obtained as a yellow powder (Yield: 0.12g, 68%). ESI-MS: *m/z* 738.10 $[\text{Rh1}-PF_6^-]^+$. ^{1}H NMR (400 MHz, DMSO-d_6) δ: 11.95 (s, 2H), 9.77 (t, 1H), 8.92 (d, 1H), 8.82 (d, 1H), 8.68 (s, 1H), 8.58 (s, 1H), 8.25 (d, 1H), 7.89 (s, 1H), 7.88—7.84 (m, 1H), 7.78 (dd, 2H), 7.72 (d, 1H), 7.44 (d, 1H), 4.77 (d, 2H), 2.69 (s, 3H), 1.66 (s, 15H). ^{13}C NMR (101 MHz, DMSO-d_6) δ: 191.76, 181.60, 165.24, 161.81, 161.57, 154.17, 153.79, 153.47, 152.85, 152.42, 151.79, 141.29, 141.14, 138.07, 134.13, 133.64, 126.49, 125.13, 124.76, 123.17, 122.40, 119.97, 118.31, 118.02, 116.50, 97.19, 21.20, 8.84.

Ru1 ($[(\eta^6\text{-p-cymene})\text{Ru(N^N-Rhein)Cl}]PF_6$) was obtained as a yellow powder (Yeild: 0.11g, 65%). ^{1}H NMR (400 MHz, DMSO-d_6) δ: 9.72 (s, 1H), 9.44 (d, 1H), 9.36 (d, 1H), 8.60 (s, 1H), 8.51 (s, 1H), 8.17 (s, 1H), 7.90 (s, 1H), 7.83—7.79 (m, 1H), 7.74 (d, 1H), 7.66 (dd, 2H), 7.41 (d, 1H), 6.19 (d, 2H), 5.94 (d, 2H), 4.75 (d, 2H), 3.17 (s, 2H), 2.59 (s, 3H), 2.33—2.26 (m, 1H), 2.15 (s, 3H), 0.95 (d, 6H).

Cell culture

A549 cells, cisplatin-resistant A549 (A549R) cells, A2780 cells and MCF-7 cells were cultured in DMEM with 10% fetal bovine serum (FBS) (10099141, Gibco) and antibiotics. NB4 cells were cultured in RPMI1640 supplemented with 10% FBS and antibiotics. All the cells were maintained in a humidified 5% CO_2 atmosphere at 37 °C.

In vitro cytotoxicity determination

Approximately 5×10^3 cells/well were seeded into 96-well plate and cultured at 37 °C for 12 h. For the adherent cell lines, the media were refreshed with indicated concentrations of the tested complexes, dimers or the ligand. After treatment for 48 h, the cell viability was determined by adding 10 μL MTT solution for 4 h. The purple product was dissolved with DMSO reagent and recorded at 490 nm with a microplate reader (Tecan Infinite M1000 Pro). For the suspension NB4 cells, the tested compounds were immediately added when cells were seeded. The CCK-8 kit (MA0218, Meilunbio) was used according to the manufacturer's instructions and the absorbance was recorded at 450 nm. Each well was in triplicate. The DMSO control was viewed as 100% and the IC_{50} value was calculated with nonlinear regression analysis using equation in GraphPad Prism 8.

Colony formation assay

A549 and A549R cells were seeded at a density of 1000 cells/well into a six-well plate and incubated at 37 °C for 12 d. The culture medium was refreshed every 3 d. Cells were fixed with 4% paraformaldehyde for 15 min and then stained with 1% crystal violet for 10 min.

Western blotting

A549 cells were seeded into 6-well plates and treated with the indicated concentrations of metal complex for 24 h at 37 °C. Cells were washed three times with PBS and lysed in RIPA Lysis Buffer with a protease inhibitor cocktail (C600387, Sangon Biotech) for 30 min on ice. The lysed cells were centrifuged at 14 000 r/min for 30 min at 4 °C, and quantified by a BCA protein assay reagent kit (P0011, Beyotime). The protein samples were separated on 12% SDS-PAGE and transferred onto nitrocellulose membranes (HATF0010, Millipore) for western blotting analysis. The primary antibodies used were FTO (ab124892, Abcam, 1 : 3000), LC3 rabbit monoclonal-antibody (AL221, Beyotime, 1 : 1000), GAPDH mouse monoclonal-antibody (60004-1-Ig, Proteintech, 1 : 5000). HRP conjugated Goat Anti-mouse (CW0103, Cwbio) or Anti-rabbit IgG (CW0102, Cwbio) was used as secondary antibody.

Fluorescence microscopy

For subcellular accumulation analysis, A549 cells were treated with 5.0 μmol/L Rh1 for 5 h and then co-incubated with 150 nmol/L Lyso-Tracker Red (LTR) or 10 μg/mL Hoechst 33342 at 37 °C for 15 min, respectively. Cells were washed with pre-chilled PBS for three times and visualized immediately with the fluorescence microscopy. The excitation wavelengths for Rh1, LTR and Hoechst 33342 were set at 405 nm, 633 nm and 357 nm, respectively. And the emission wavelength was 600 ± 20 nm for Rh1, 660 ± 20 nm for LTR and 460 ± 20 nm for Hoechst 33342, respectively.

For LC3 immunofluorescence analysis, A549 cells were seeded into 35 mm dishes and treated with 10 μmol/L Rh1 or DMSO for 12 h, followed by washing twice with the serum-free medium. Then cells were fixed with 3.7% formaldehyde solution for 15 min and washed with a PBS solution containing 0.2% TritonX-100 for another 15 min. Liquid was discarded and pre-diluted anti-LC3B rabbit antibody (ab48394, Abcam) was incubated to cells for 2 h at room temperature. After incubation and washing, the FITC-labelled goat anti-rabbit IgG was added at 37 °C for another 1 h. The supernatant was removed and the cells were stained with Hoechst 33342 for another 15 min. After washing twice with PBS, cells were observed immediately by fluorescence microscopy with the excitation wavelength set at 488 nm for FITC and 357 nm for Hoechst 33342. The emission wavelength was 530 ± 20 nm for FITC and 460 ± 20 nm for Hoechst 33342, respectively.

ROS detection

A549 cells were seeded into 35 mm dishes and treated with the Rh1 complexes at required concentrations for different time points. The detection of ROS was performed in accordance with the manufacturer's instructions (KGAF018, KeyGEN BioTECH). Briefly, cells were stained with 10 μmol/L H2DCFDA in the dark for 30 min, and washed with PBS for three times to discard the dye solutions. The fluorescence intensity was measured immediately by the fluorescence microscopy or fluorescence spectrometer with an excitation wavelength at 488 nm and an emission wavelength at 530 ± 30 nm.

Cell cycle analysis

The cell cycle analysis was conducted as the manufacturer's

protocol (KGA512, KeyGEN BioTECH). A549 cells were cultured in 6-well plates and incubated with Rh1 (0, 0.5, 2.5, 5 μmol/L, respectively) for 24 h. Cells were collected and fixed 70% ethanol. After storage at 4 °C overnight, cells were centrifuged and washed three times with cold PBS and resuspended in a 500 μL PBS buffer containing PI and RNase A (9 : 1) for 30 min in the dark. The samples were analyzed by a flow cytometry and the data were processed using the ModFit LT 2.0 software (Verity Software House, USA).

Protein expression and purification

The N-terminal 31 residues truncated FTO gene was subcloned into pET28a vector, encoding a His-tag fusion FTO protein. The expression and purification of FTO were modified from previously reported methods.[37] The protein was purified by Nickle-affinity chromatography, followed by a superdex 200 gel filtration (GE Healthcare). Fractions were collected and checked by 12% SDS-PAGE. The proteins were stored at –80 °C for further bioassays.

Inhibition of FTO demethylation *in vitro*

The PAGE-based assay for inhibition of FTO demethylation *in vitro* was performed as previously described.[37-38] A reaction mixture, containing 0.5 μmol/L FTO, 1 μmol/L 39-nt ssDNA (5'-ATTGCCATTCTCGATAGG(m^6A)TCCGGTCAAACCTAGACGAA-3'), 300 μmol/L α-ketoglutarate, 280 μmol/L $(NH_4)_2Fe(SO_4)_2$, 2 mmol/L *L*-ascorbic acid and inhibitors at required concentrations in 50 mmol/L Tris-HCl, pH 7.5, was incubated at room temperature for 2 h. The reaction was terminated by heating at 65 °C for 15 min. The ssDNA was annealed to the complementary strand and then subjected to the DpnII enzyme digestion (R0543L, NEB). The digested dsDNA was checked on 15% native PAGE with GelRed staining to estimate the percentage of inhibition.

RNA extraction and m^6A dot blot

A549 cells were incubated with indicated concentrations of Rh1 for 48 h. Total RNA was extracted with TRIzol reagents (15596018, Thermofisher Scientific) and mRNA was then isolated from total RNA using Dynabeads mRNA DIRECT kit (61012, Thermofisher Scientific) in accordance with the manufacturer's protocols. RNA samples were denatured and then spotted onto an Immobilon-Ny + membrane (INYC00010, Millipore). After complete drying, RNA samples were crosslinked by an UV irradiation for 3 min. The membrane was then blocked with 5% non-fat dry milk in 1×PBST buffer for 1 h at room temperature and subsequently incubated with rabbit anti-m^6A antibody (ab151230, Abcam) at 4 °C overnight. After three washes with PBST, the membrane was incubated with anti-rabbit IgG antibody for 1 h at room temperature, then washed for another three times in PBST. Finally, the membrane was developed with Amersham ECL Prime Western Blotting Detection Reagent (RPN2232, GE Healthcare) and stained with 0.1% methylene blue (MB) as loading control.

Stable cell line generation

Lentivirus was generated as described previously.[31] Briefly, 1.5 μg pMD2.G, 0.9 μg pMDLg/pRRE, 2.1 μg pRSV-Rev, and 5.4 μg shRNA plasmids pLKO.1-shFTO or pLKO.1-shNC constructs were co-transfected into HEK293T/17 cells with the Lipo2000 transfection reagent (11668500, ThermoFisher) according to the manufacturer's instructions. The target sequences for FTO knockdown were listed in Table S2. The lentivirus particles were harvested 48 h and 72 h post transfection, directly pipetted into A549 cells in the presence of 6 μg/mL polybrene (H9268, Sigma-Aldrich). Finally, 5 μg/mL puromycin (P8833, Sigma-Aldrich) was added into the A549 cells 48 h post incubation to select the positive infected-cells. To avoid cellular compensation of knockdown efficiency, only freshly infected cell lines (fewer than 6 passages) were used in the experiments.

Supporting Information

The supporting information for this article is available on the WWW under https://doi.org/10.1002/cjoc.202100901.

Acknowledgement

We thank NSFC (Nos. 22077066, 21771109, 21778033, 21701195, 21837006, 21977052 and 21907101).

References

[1] Ko, C.-N.; Li, G.; Leung, C.-H.; Ma, D.-L. Dual function luminescent transition metal complexes for cancer theranostics: The combination of diagnosis and therapy. *Coord. Chem. Rev.* **2019**, *381*, 79–103.

[2] Rosenberg, B.; Van Camp, L.; Krigas, T. Inhibition of Cell Division in Escherichia coli by Electrolysis Products from a Platinum Electrode. *Nature* **1965**, *205*, 698–699.

[3] Peng, K.; Liang, B.-B.; Liu, W.; Mao, Z.-W. What blocks more anticancer platinum complexes from experiment to clinic: Major problems and potential strategies from drug design perspectives. *Coord. Chem. Rev.* **2021**, *449*, 214210.

[4] Zhu, X.; Su, Q.; Feng, W.; Li, F. Anti-Stokes shift luminescent materials for bio-applications. *Chem. Soc. Rev.* **2017**, *46*, 1025–1039.

[5] Bergamo, A.; Gaiddon, C.; Schellens, J. H.; Beijnen, J. H.; Sava, G. Approaching tumour therapy beyond platinum drugs: status of the art and perspectives of ruthenium drug candidates. *J. Inorg. Biochem.* **2012**, *106*, 90–99.

[6] Yousuf, I.; Bashir, M.; Arjmand, F.; Tabassum, S. Advancement of metal compounds as therapeutic and diagnostic metallodrugs: Current frontiers and future perspectives. *Coord. Chem. Rev.* **2021**, *445*, 214104.

[7] Das, U.; Kar, B.; Pete, S.; Paira, P. Ru(ii), Ir(iii), Re(i) and Rh(iii) based complexes as next generation anticancer metallopharmaceuticals. *Dalton Trans*. **2021**, *50*, 11259–11290.

[8] Liu, H.-K.; Sadler, P. J. Metal Complexes as DNA Intercalators. *Acc. Chem. Res.* **2010**, *44*, 349–359.

[9] Liu, H.-K.; Berners-Price, S. J.; Wang, F.; Parkinson, J. A.; Xu, J.; Bella, J.; Sadler, P. J. Diversity in Guanine-Selective DNA Binding Modes for an Organometallic Ruthenium Arene Complex. *Angew. Chem. Int. Ed.* **2006**, *118*, 8333–8336.

[10] Lomzik, M.; Hanif, M.; Budniok, A.; Blauz, A.; Makal, A.; Tchon, D. M.; Lesniewska, B.; Tong, K. K. H.; Movassaghi, S.; Sohnel, T.; Jamieson, S. M. F.; Zafar, A.; Reynisson, J.; Rychlik, B.; Hartinger, C. G.; Plazuk, D. Metal-Dependent Cytotoxic and Kinesin Spindle Protein Inhibitory Activity of Ru, Os, Rh, and Ir Half-Sandwich Complexes of Ispinesib-Derived Ligands. *Inorg. Chem.* **2020**, *59*, 14879–14890.

[11] Zhang, S.; Zhong, X.; Yuan, H.; Guo, Y.; Song, D.; Qi, F.; Zhu, Z.; Wang, X.; Guo, Z. Interfering in apoptosis and DNA repair of cancer cells to conquer cisplatin resistance by platinum(iv) prodrugs. *Chem. Sci.* **2020**, *11*, 3829–3835.

[12] Casini, A.; Gabbiani, C.; Sorrentino, F.; Rigobello, M. P.; Bindoli, A.; Geldbach, T. J.; Marrone, A.; Re, N.; Hartinger, C. G.; Dyson, P. J.; Messori, L. Emerging Protein Targets for Anticancer Metallodrugs Inhibition of Thioredoxin Reductase. *J. Inorg. Biochem.* **2008**, *51*, 6773–6881.

[13] Meier, S. M.; Kreutz, D.; Winter, L.; Klose, M. H. M.; Cseh, K.; Weiss, T.; Bileck, A.; Alte, B.; Mader, J. C.; Jana, S.; Chatterjee, A.; Bhattacharyya, A.; Hejl, M.; Jakupec, M. A.; Heffeter, P.; Berger, W.; Hartinger, C. G.; Keppler, B. K.; Wiche, G.; Gerner, C. An Organoruthenium Anticancer Agent Shows Unexpected Target Selectivity For Plectin. *Angew. Chem. Int. Ed.* **2017**, *56*, 8267–8271.

[14] Kaur, M.; Loveleen; Kumar, R. Inhibition of histone deacetylases, topoisomerases and epidermal growth factor receptor by metal-

based anticancer agents: Design & synthetic strategies and their medicinal attributes. *Bioorg. Chem.* **2020**, *105*, 104396.

[15] Srivastava, P.; Verma, M.; Kumar, A.; Srivastava, P.; Mishra, R.; Sivakumar, S.; Patra, A. K. Luminescent naphthalimide-tagged ruthenium(ii)-arene complexes: cellular imaging, photocytotoxicity and transferrin binding. *Dalton Trans*. **2021**, *50*, 3629–3640.

[16] Qiu, K.; Chen, Y.; Rees, T. W.; Ji, L.; Chao, H. Organelle-targeting metal complexes: From molecular design to bio-applications. *Coord. Chem. Rev.* **2019**, *378*, 66–86.

[17] He, L.; Li, Y.; Tan, C. P.; Ye, R. R.; Chen, M. H.; Cao, J. J.; Ji, L. N.; Mao, Z. W. Cyclometalated iridium(iii) complexes as lysosome-targeted photodynamic anticancer and real-time tracking agents. *Chem. Sci.* **2015**, *6*, 5409–5418.

[18] Gupta, G.; Kumari, P.; Ryu, J. Y.; Lee, J.; Mobin, S. M.; Lee, C. Y. Mitochondrial Localization of Highly Fluorescent and Photostable BODIPY-Based Ruthenium(II), Rhodium(III), and Iridium(III) Metal Complexes. *Inorg. Chem.* **2019**, *58*, 8587–8595.

[19] Xue, X.; Qian, C.; Tao, Q.; Dai, Y.; Lv, M.; Dong, J.; Su, Z.; Qian, Y.; Zhao, J.; Liu, H. K.; Guo, Z. Using bio-orthogonally catalyzed lethality strategy to generate mitochondria-targeting anti-tumor metallodrugs in vitro and in vivo. *Natl. Sci. Rev.* **2021**, *8*, nwaa 286.

[20] Xue, X.; Qian, C.; Fang, H.; Liu, H. K.; Yuan, H.; Guo, Z.; Bai, Y.; He, W. Photoactivated Lysosomal Escape of a Monofunctional Pt(II) Complex Pt-BDPA for Nucleus Access. *Angew. Chem. Int. Ed.* **2019**, *58*, 12661–12666.

[21] Chen, B.; Ye, F.; Yu, L.; Jia, G.; Huang, X.; Zhang, X.; Peng, S.; Chen, K.; Wang, M.; Gong, S.; Zhang, R.; Yin, J.; Li, H.; Yang, Y.; Liu, H.; Zhang, J.; Zhang, H.; Zhang, A.; Jiang, H.; Luo, C.; Yang, C.-G. Development of Cell-Active N^6-Methyladenosine RNA Demethylase FTO Inhibitor. *J. Am. Chem. Soc*. **2012**, *134*, 17963–17971.

[22] Jia, G.; Fu, Y.; Zhao, X.; Dai, Q.; Zheng, G.; Yang, Y.; Yi, C.; Lindahl, T.; Pan, T.; Yang, Y.-G.; He, C. N^6-Methyladenosine in nuclear RNA is a major substrate of the obesity-associated FTO. *Nat. Chem. Biol.* **2011**, *7*, 885–887.

[23] Galluzzi, L.; Green, D. R. Autophagy-Independent Functions of the Autophagy Machinery. *Cell* **2019**, *177*, 1682–1699.

[24] Runwal, G.; Stamatakou, E.; Siddiqi, F. H.; Puri, C.; Zhu, Y.; Rubinsztein, D. C. LC3-positive structures are prominent in autophagy-deficient cells. *Sci. Rep.* **2019**, *9*, 10147.

[25] Kwon, N.; Kim, D.; Swamy, K. M. K.; Yoon, J. Metal-coordinated fluorescent and luminescent probes for reactive oxygen species (ROS) and reactive nitrogen species (RNS). *Coord. Chem. Rev.* **2021**, *427*, 213581.

[26] Cheng, F.; Huang, L.; Wang, H.; Liu, Y.; Kandhadi, J.; Wang, H.; Ji, L.; Liu, H. Photodynamic Therapy Activities of 10-(4-Formylphenyl)-5,15-bis(pentafluorophenyl)corrole and Its Gallium Complex. *Chin. J. Chem.* **2017**, *35*, 86–92.

[27] Zheng, K.; He, Z.; Kitazato, K.; Wang, Y. Selective Autophagy Regulates Cell Cycle in Cancer Therapy. *Theranostics* **2019**, *9*, 104–125.

[28] Shi, H.; Zhao, J.; Han, L.; Xu, M.; Wang, K.; Shi, J.; Dong, Z. Retrospective study of gene signatures and prognostic value of m6A regulatory factor in non-small cell lung cancer using TCGA database and the verification of FTO. *Aging-US* **2020**, *12*, 17022–17037.

[29] Ding, Y.; Qi, N.; Wang, K.; Huang, Y.; Liao, J.; Wang, H.; Tan, A.; Liu, L.; Zhang, Z.; Li, J.; Kong, J.; Qin, S.; Jiang, Y. FTO Facilitates Lung Adenocarcinoma Cell Progression by Activating Cell Migration Through mRNA Demethylation. *Onco Targets Ther.* **2020**, *13*, 1461–1470.

[30] Zhou, L. L.; Xu, H.; Huang, Y.; Yang, C. G. Targeting the RNA demethylase FTO for cancer therapy. *RSC Chem. Biol.* **2021**, *2*, 1352–1369.

[31] Huang, Y.; Su, R.; Sheng, Y.; Dong, L.; Dong, Z.; Xu, H.; Ni, T.; Zhang, Z. S.; Zhang, T.; Li, C.; Han, L.; Zhu, Z.; Lian, F.; Wei, J.; Deng, Q.; Wang, Y.; Wunderlich, M.; Gao, Z.; Pan, G.; Zhong, D.; Zhou, H.; Zhang, N.; Gan, J.; Jiang, H.; Mulloy, J. C.; Qian, Z.; Chen, J.; Yang, C. G. Small-Molecule Targeting of Oncogenic FTO Demethylase in Acute Myeloid Leukemia. *Cancer Cell* **2019**, *35*, 677–691.

[32] Su, R.; Dong, L.; Li, Y.; Gao, M.; Han, L.; Wunderlich, M.; Deng, X.; Li, H.; Huang, Y.; Gao, L.; Li, C.; Zhao, Z.; Robinson, S.; Tan, B.; Qing, Y.; Qin, X.; Prince, E.; Xie, J.; Qin, H.; Li, W.; Shen, C.; Sun, J.; Kulkarni, P.; Weng, H.; Huang, H.; Chen, Z.; Zhang, B.; Wu, X.; Olsen, M. J.; Muschen, M.; Marcucci, G.; Salgia, R.; Li, L.; Fathi, A. T.; Li, Z.; Mulloy, J. C.; Wei, M.; Horne, D.; Chen, J. Targeting FTO Suppresses Cancer Stem Cell Maintenance and Immune Evasion. *Cancer Cell*. **2020**, *38*, 1–18.

[33] Liu, Y.; Liang, G.; Xu, H.; Dong, W.; Dong, Z.; Qiu, Z.; Zhang, Z.; Li, F.; Huang, Y.; Li, Y.; Wu, J.; Yin, S.; Zhang, Y.; Guo, P.; Liu, J.; Xi, J. J.; Jiang, P.; Han, D.; Yang, C. G.; Xu, M. M. Tumors exploit FTO-mediated regulation of glycolytic metabolism to evade immune surveillance. *Cell Metab.* **2021**, *33*, 1–13.

[34] Zheng, Y.; Ling, Y.; Zhang, D. Y.; Tan, C. P.; Zhang, H.; Yang, G. G.; Wang, H.; Ji, L. N.; Mao, Z. W. Regulating Tumor N(6)-Methyladenosine Methylation Landscape using Hypoxia-Modulating OsSx Nanoparticles. *Small* **2021**, *17*, e2005086.

[35] Ashford, D. L.; Stewart, D. J.; Glasson, C. R.; Binstead, R. A.; Harrison, D. P.; Norris, M. R.; Concepcion, J. J.; Fang, Z.; Templeton, J. L.; Meyer, T. J. An amide-linked chromophore-catalyst assembly for water oxidation. *Inorg. Chem.* **2012**, *51*, 6428–6430.

[36] Chen, J.; Tao, Q.; Wu, J.; Wang, M.; Su, Z.; Qian, Y.; Yu, T.; Wang, Y.; Xue, X.; Liu, H. K. A lysosome-targeted ruthenium(II) polypyridyl complex as photodynamic anticancer agent. *J. Inorg. Biochem.* **2020**, *210*, 111132.

[37] Huang, Y.; Yan, J.; Li, Q.; Li, J.; Gong, S.; Zhou, H.; Gan, J.; Jiang, H.; Jia, G. F.; Luo, C.; Yang, C. G. Meclofenamic acid selectively inhibits FTO demethylation of m6A over ALKBH5. *Nucleic Acids Res.* **2015**, *43*, 373–384.

[38] Wang, T. L.; Hong, T. T.; Huang, Y.; Su, H. M.; Wu, F.; Chen, Y.; Wei, L.; Huang, W.; Hua, X. L.; Xia, Y.; Xu, J. L.; Gan, J. H.; Yuan, B. F.; Feng, Y. Q.; Zhang, X. L.; Yang, C. G.; Zhou, X. Fluorescein Derivatives as Bifunctional Molecules for the Simultaneous Inhibiting and Labeling of FTO Protein. *J. Am. Chem. Soc*. **2015**, *137*, 13736–13739.

Manuscript received: December 20, 2021
Manuscript revised: January 17, 2022
Manuscript accepted: January 19, 2022
Accepted manuscript online: January 25, 2022
Version of record online: February 12, 2022

The Authors

First Row: (left to right) Lu Liu, Yaqiong Kong, Hong-Jiao Xu, Liang He, Zong-Wan Mao, Hong-Ke Liu

Second Row: (left) Xiu-Xiu Wang, Jing Zhao, (middle) Yue Huang, Cai-Guang Yang, (right) Meng-Meng Wang, Zhi Su